ADVANCED FUNCTIONAL MATERIALS
www.afm-journal.de

Sub-Band Filling and Hole Transport in Polythiophene-Based Electrolyte-Gated Transistors: Effect of Side-Chain Length and Density

Kyung Gook Cho, Demetra Z. Adrahtas, Keun Hyung Lee, and C. Daniel Frisbie**

The relationship between hole density and conductivity in electrochemically gated polythiophene films is examined. The films are integrated into electrolyte-gated transistors (EGTs), so that hole accumulations can be electrochemically modulated up to ≈0.4 holes per thiophene ring (hpr). Polythiophenes include poly(3-alkylthiophenes) (P3ATs) with four different side chain lengths – butyl (P3BT), hexyl (P3HT), octyl (P3OT), or decyl (P3DT) – and poly[2,5-bis(3-dodecylthiophen-2-yl)thieno[3,2-*b*]thiophene] (PBTTT) and poly(3,3‴-didodecyl[2,2′:5′,2″:5″,2‴-quaterthiophene]-5,5‴-diyl) (PQT). Analysis of the drain current – gate voltage (I_D–V_G) and gate current – gate voltage (I_G–V_G) characteristics of the EGTs reveals that all six polythiophene semiconductors exhibited reversible conductivity peaks at 0.12 – 0.15 hpr. Conductivity is suppressed beyond ≈0.4 hpr.The maximum carrier mobilities of the P3AT semiconductors increase, and hysteresis of the conductivity peaks decreases, with increasing alkyl side-chain length. PBTTT and PQT with reduced side chain densities exhibit the largest hysteresis but have higher hole mobilities. The results suggest that at ≈0.4 hpr, a polaronic sub-band is filled in all cases. Filling of the sub-band correlates with a collapse in the hole mobility. The side-chain dependence of the peak conductivity and hysteresis further suggests that Coulombic ion-carrier interactions are important in these systems. Tailoring ion-carrier correlations is likely important for further improvements in transport properties of electrochemically doped polythiophenes.

1. Introduction

Electrolyte-gated transistors (EGTs) based on conjugated polymer semiconductors have attracted significant interest for applications in flexible/stretchable, bioelectronic, and neuromorphic devices.[1–4] An intriguing feature of EGT systems is the penetration of electrolyte ions into the conjugated polymer semiconductor to form a 3D ionic/electronic conduction channel. In this mixed conduction channel, carrier accumulations can be extremely large (>10^{21} cm^{-3}), allowing EGTs and their logic circuits to operate at low voltages with a high channel current and ON/OFF current ratio.[4] Understanding carrier accumulation and transport in these mixed ionic/electronic channels is important because they not only determine the major EGT characteristics, such as threshold voltage, transconductance, mobility (μ), and stability, but also pave the way for future electrochemical and electronic applications, such as human-machine interfaces, electrochromic displays, artificial synapses, and soft-robotics.[5–13] Accordingly,significant effort has been devoted to understanding the physical principles and mechanisms underlying the ionic/electronic mixed conduction by investigating ion doping/de-doping, morphology changes, charge carrier accumulation and transport, and ionic-electronic coupling.[11,12,14–22] However, a complete physical picture of these complex phenomena has yet to be developed.

In conventional polymer thin film transistors, the electrical conductivity of conjugated polymers increases as the carrier concentration increases. In contrast, in polymer EGTs, which accumulate charge carriers by electrochemical doping, a conductivity peak is often observed with increasing carrier density.[23–25] This phenomenon was first demonstrated by Wrighton and colleagues in the 1980s and 1990s.[26,27] They showed that electrochemically doped polymer semiconductors, including polythiophenes, polypyrroles, and polyaniline, exhibited clear conductivity peaks as a function of gate voltage. The conductivity peaks were reversible and reproducible: multiple drain current–gate voltage (I_D–V_G) sweeps showed the same behavior, indicating

K. G. Cho, K. H. Lee
Department of Chemistry and Chemical Engineering
Education and Research Center for Smart Energy and Materials
Inha University
Incheon 22212, Republic of Korea
E-mail: kh.lee@inha.ac.kr
D. Z. Adrahtas, C. D. Frisbie
Department of Chemical Engineering and Materials Science
University of Minnesota–Twin Cities
Minneapolis, Minnesota 55455, United States
E-mail: frisbie@umn.edu
The ORCID identification number(s) for the author(s) of this article can be found under https://doi.org/10.1002/adfm.202303700

DOI: 10.1002/adfm.202303700

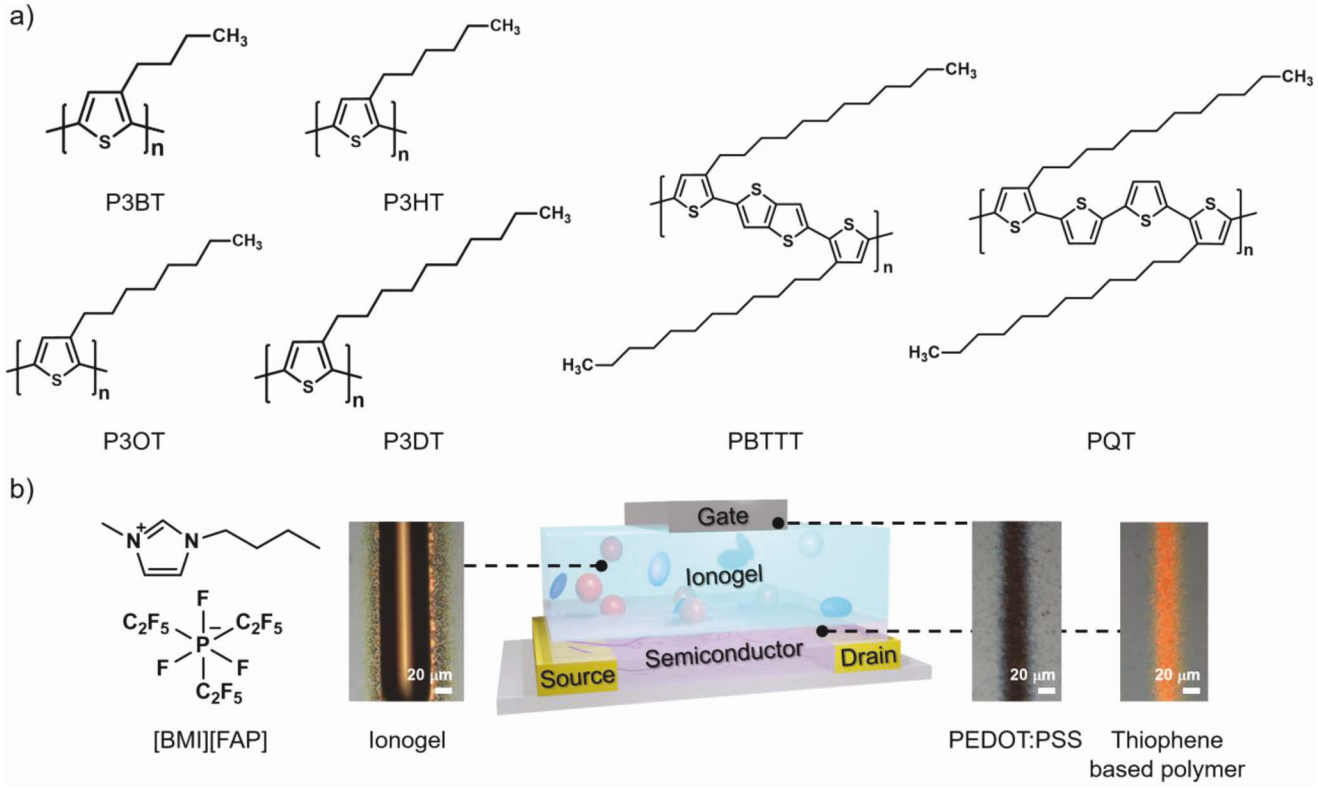

Figure 1. a) Chemical structures of the thiophene-based semiconductors with different chain architecture: P3BT, P3HT, P3OT, P3DT, PBTTT, and PQT. b) Schematic of an aerosol-jet-printed EGT with a bottom-contact/top-gated structure. Thiophene-based polymer semiconductors, the ionogel based on [BMI][FAP] ionic liquid and a block polymer, and PEDOT:PSS were printed as the channel, gate dielectric, and gate electrode, respectively.

that the collapse of conductivity at high V_G was not due to sample degradation. Similar results have been reported by us and by Fabiano, Kemerink, and co-workers using various p- and n-type semiconductors.[6,23–25,28–31]

The physical origins of the conductivity peaks might be Coulombic interactions between ions and carriers that inhibit the transport of free-carriers. Interactions between ions and charge carriers, and their effects on ionic/electronic mixed conduction have been studied previously.[6,11,12,17,32–34] In particular, some of us recently demonstrated that the conductivity versus surface carrier density behavior in an n-type C_{60} single crystal EGT depends on the size of the electrolyte ions.[6] In particular, small cations in the gate electrolyte were found to interact more strongly with electrons in the C_{60} channel and localize the carriers, favoring activated hopping transport; whereas, larger cations allowed delocalization of electrons, leading to band-like transport. The cation radius dependence on transport in that study demonstrated that ion-carrier interactions are important and that Coulomb forces, specifically, are likely the cause.

In this study, we focus on ion-carrier interactions and hole transport behavior in EGTs based on p-type polythiophenes, **Figure 1**. Instead of varying ion radius in the gate electrolyte as in the C_{60} experiment just described, we have kept the cation-anion composition in the electrolyte constant, and have chosen six different polythiophenes that have systematically varied alkyl side chain lengths or alkyl side chain density, Figure 1a. The idea is that the different side chain lengths and side chain densities will present tunable steric barriers between anions in the electrolyte and electrochemically induced holes in the polymer pi-conjugated backbones, ultimately tuning the anion-hole interaction.

The EGT devices, shown in Figure 1b, were fabricated using aerosol jet printing to deposit the polythiophene channel materials, the ionogel gate electrolyte, and the conducting polymer gate electrode with uniform thicknesses. These devices were then employed to measure the electronic conductivities of each of the polymers as a function of gate-controlled hole density up to and beyond ~0.4 holes per thiophene ring (hpr). Our main findings are: (i) all polymers exhibited conductivity peaks versus hole density with the peak maximum occurring at 0.12 – 0.15 hpr; (ii) conductivity was completely shut off beyond 0.32 – 0.38 hpr for all cases; (iii) for the poly(3-alkylthiophene) series, the value of the peak conductivity (and thus average peak mobility) systematically increased with increasing side chain length; and (iv) all polymers exhibited hysteresis in the conductivity peak between forward and reverse gate voltage sweeps and the magnitude of the hysteresis was correlated with side-chain steric hindrance. Collectively, these results expand the number of examples in the literature demonstrating the peaked dependence of conductivity on charge density in organic conductors. They also support the interpretation that ion-carrier interactions are critical to carrier transport in these systems. We discuss the results in terms of the interplay of the evolving electronic density of states upon electrochemical doping and the role of ion-carrier interactions on hole

localization and delocalization. Further improvements in hole conductivity in p-type polymer EGTs will likely require expanded efforts to minimize anion-hole interactions.

2. Results and Discussion

Figure 1b and Figure S1 (Supporting Information) show the scheme of a bottom-contact/top-gated EGT and aerosol-jet-printed ionogel dielectric, poly(3,4-ethylenedioxythiophene):poly(styrenesulfonate) (PEDOT:PSS) gate electrode, and thiophene-based polymer semiconductor. The active materials of the EGTs were sequentially deposited on the Au S/D channels with controlled thicknesses and areas. Thiophene-based *p*-type semiconductors, including poly(3-alkylthiophenes) (P3AT) with butyl (P3BT), hexyl (P3HT), octyl (P3OT), or decyl (P3DT) side chains, poly[2,5-bis(3-dodecylthiophen-2-yl)thieno[3,2-b]thiophene] (PBTTT), and poly(3,3‴-didodecyl[2,2′:5′,2″:5″,2‴-quaterthiophene]-5,5‴-diyl) (PQT), Figure 1a, were successfully aerosol-jet-printed on the EGT channels with an average thickness of 52 ± 7 nm (see Figures S1a and S2, Supporting Information). For the ionogel dielectric, a 1-butyl-3-methylimidazolium tris(pentafluoroethyl)trifluorophosphate ([BMI][FAP]) ionic liquid (IL) and a gelating poly(styrene-*b*-ethyl acrylate-*b*-styrene) (SEAS) triblock polymer consisting of IL-insoluble polystyrene end blocks, and an IL-soluble poly(ethyl acrylate) midblock, were utilized.[35]

Figure 2a,b shows the corresponding I_D-V_G behaviors on semi-log and linear axes, respectively, of a P3HT EGT up to V_G = −5 V at fixed V_D = −0.1 V. The device turns ON at negative V_G values which is indicative of hole (p-type) transport. A clear conductivity peak is evident in both plots; the channel current I_D peaks at ≈−0.1 mA at V_G = −1.7 V and then decreases as V_G becomes more negative. I_D–V_D output curves presented in Figure S3 (Supporting Information) also confirm the conductivity peak occurs at high V_G values; the I_D at V_G = −2.5 V is smaller than that at V_G = −1.5 V. The conductivity peak is reversible, albeit with hysteresis; reversing the V_G sweep direction (positive-going) results in a peak that is not as tall as the forward (negative-going) sweep and it is shifted to more positive potentials by +450 mV. However, multiple consecutive sweeps demonstrate that both conductivity peaks on forward and reverse scans are reproducible, **Figure 2**b. The peaked behavior does not represent chemical degradation but is the result of reversible electrochemical charging/discharging of carriers in the semiconductor channel. In spite of the reversible charging/discharging, the maximum conductivity for forward and backward directions slightly decreases after 10 cycles. This might come from the residual impurities in the [BMI][FAP] such as water or halides, which can reduce the electrochemical stability of the IL.[36–38]

The corresponding I_G–V_G (charging current) characteristic in Figure 2c shows the reversible charging and discharging of the P3HT channel directly. Negative I_G currents on sweeping V_G in the negative direction correspond to hole accumulation in the P3HT and positive I_G values on sweeping V_G positively correspond to hole depletion. The pronounced charging and discharging peaks evident in Figure 2c are intriguing; they indicate that carrier accumulation is essentially shut down at large negative V_G values. Comparison of Figure 2a–c also shows that the peak

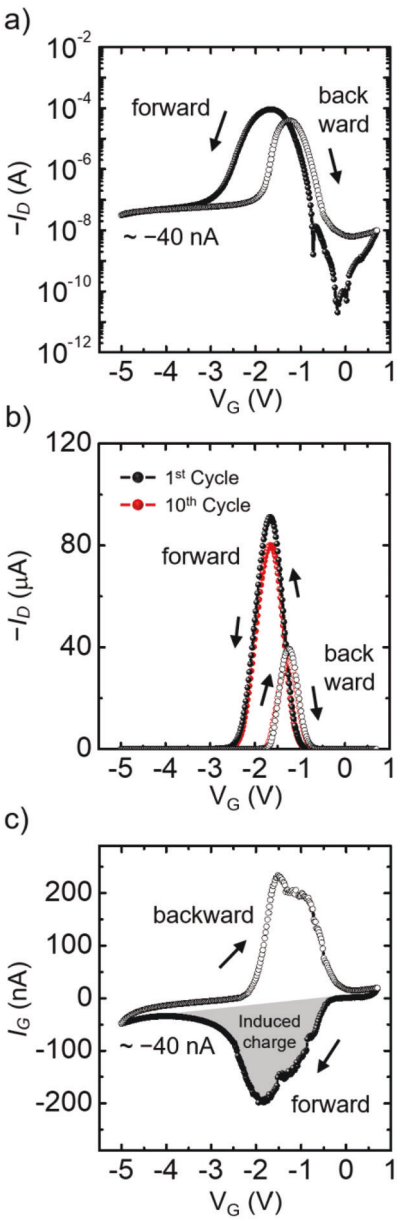

Figure 2. a) Semi-log and b) linear I_D–V_G transfer characteristics for a P3HT EGT with V_D = −0.1 V. c) I_G-V_G charging/discharging curves for the same P3HT EGT. The solid and open symbols denote forward and backward sweep directions in all panels. All EGT measurements were taken with a V_G scan rate of 50 mV s^{-1} at room temperature and under a nitrogen atmosphere.

in I_G is well matched to the peak in I_D, and, like the I_D–V_G characteristics, the I_G–V_G traces are reversible with hysteresis in the peak position.

It is well-established that the I_G–V_G characteristic reflects the evolving electronic density of states during electrochemical doping of polymer semiconductors, and it can be integrated to give the total carrier accumulation as a function of V_G.[23,25] However, essentially complete suppression of carrier accumulation beyond a certain V_G value is not commonly reported.[6] We believe that the forward I_G–V_G trace in Figure 2c essentially represents

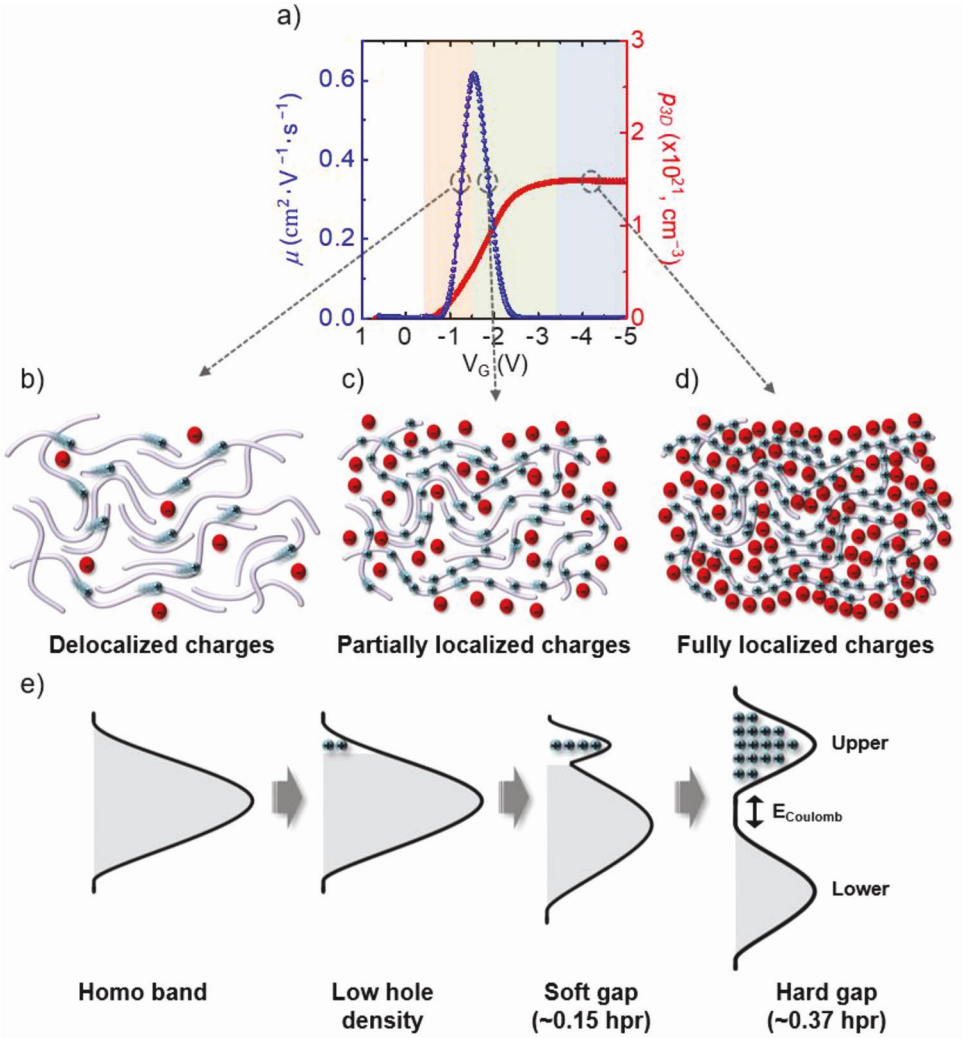

Figure 3. a) Charge carrier mobility and volumetric density as a function of V_G for a P3HT EGT. b–d) are schematics depicting electrochemically induced holes (blue circles) and counter ions (red circles) at different charge densities. Delocalization and localization of the holes are indicated by the smearing of the blue circles. e) Evolution of the density of states with increasing hole density on the thiophene polymer.

filling of an electronic sub-band (a polaron band) in the density of states of the P3HT with polaronic holes, and that the reverse trace corresponds to depletion of holes from this sub-band. This will be discussed further below. For now, we would like to point out that our ability to scan to large V_G values, which is necessary to fill the band, reflects our choice of electrolyte and gate electrode. The IL that composes the ionogel is well known to have a wide electrochemical window, far greater than the window in aqueous electrolytes (≈1.23 V) which is limited by water electrolysis.[39] The PEDOT:PSS gate electrode also represents a permeable, 3D, high capacitance contact to the electrolyte, which means that voltage drop at the gate/electrolyte interface is minimized.[40] When we made EGTs using Au gate electrodes, we were not able to achieve stable and reproducible I_D–V_G and I_G–V_G sweeps out to large gate voltages (Figure S4, Supporting Information). We believe this was due to the smaller effective surface area, and thus smaller capacitance of the Au/electrolyte interface, which lead to high voltage drops at that interface and less overall gating power.

Figure 3a displays the average carrier mobility and volumetric charge density in P3HT EGTs as functions of V_G, extracted from the data in Figure 2 using Equations 1–3. The hole mobility and hole density exhibit very different trends. Hole density increases to 1.5×10^{21} cm^{-3} (0.37 hpr) and then essentially plateaus, reflecting the peak in the I_G–V_G behavior. Average hole mobility (Equation 3), on the other hand, increases with V_G and peaks at $V_G \approx -1.5$ V, corresponding to a hole density of 0.60×10^{21} cm^{-3} or 0.14 hpr. It's clear from this analysis that the peak in the I_D–V_G (transconductance) characteristic reflects the peaked behavior of mobility with carrier density, not the carrier density itself, which levels off.[6,23] The initial mobility increase at a low carrier density is typical in organic systems and is probably due to the filling of carrier traps and carrier-induced structural changes in the polymer that delocalize the holes.[23] We propose that holes are loosely coupled to electrolyte ions at this stage (light orange shaded region in Figure 3a). At the mobility peak, carrier localization effects begin which lower the mobility as more charge is added to the system (green shaded region in Figure 3a). The localization

effects conceivably have two principal causes: (1) hole-hole interactions,[31] as the carrier density is high, and (2) hole-ion interactions, shown schematically in Figure 3b–d. Coulomb repulsion between holes at the maximum mobility peak is estimated to be ≈50 meV, or approximately twice the thermal energy. For this calculation, the dielectric constant of the P3HT/IL composite was taken to be ≈10 even though un-doped polythiophenes generally have a low dielectric constant of 3–4. The value of 10 is rationalized in that [BMI]-based ILs have a dielectric constant of ∼10 at room temperature and electrochemical doping is known to make polythiophenes more polarizable.[41–43] It seems from this rough estimate that hole-hole interactions are important, especially as the hole density increases beyond 0.14 hpr.

However, our focus here is on the possibility of hole-anion interactions as a cause of carrier localization, as our selection of semiconducting polymers with different side chain lengths and side-chain densities provides a way to tune average hole-anion separations via steric interactions. As the hole density in P3HT increases to the peak mobility and beyond, we propose that anions begin to localize holes on the P3HT chains by Coulomb attraction, Figure 3c. Eventually, at the highest charge densities of 1.5×10^{21} cm^{-3}, or 0.37 holes per monomer, a hard Coulomb gap develops in the density of states and the HOMO band is split into Mott-Hubbard-like upper and lower polaron bands, Figure 3e. The cause of this Coulomb gap is a combination of hole-hole repulsion and hole-anion attraction. The fact that the I_G–V_G characteristic indicates band-filling at charge densities of 0.37 hpr supports this sub-band picture. The full HOMO band should allow up to 2 hpr and the observation that band-filling occurs at 0.37 hpr, a factor of ≈5 times lower hole density than the theoretical maximum, is consistent with the presence of sub-bands. We note that Fabiano, Kemerink, and colleagues have made a similar proposal for the presence of sub-bands in an n-type polymer EGT.[30,31]

Our picture then is that the upper polaron sub-band is completely filled at ≈0.37 hpr. We estimate that both the hole-anion attraction and hole-hole repulsion will be several hundred meVs, respectively, at this charge density, which is more than $10k_BT$ and thus large enough to create a hard Coulomb gap in the density of polaronic states. The polaronic holes are locked up on the P3HT chains at charge densities of 0.37 per monomer and greater, and thus conductivity collapses.

The development of the Coulomb gap between the polaronic sub-bands will naturally depend on charge density. We propose that initially a soft gap opens precisely at the point of maximum charge mobility and that it widens and becomes the hard gap just discussed as gate-induced charge density increases, Figure 3e. Further, it is well known that the crystalline (ordered) and amorphous (disordered) domains exhibit different oxidation potentials,[19,44] and there may be different Coulomb gaps for the two domains. In our case, due to the use of low boiling point chloroform as the solvent and the absence of any post-annealing process, we anticipate that the semiconductor films studied here are mostly amorphous, and thus the effect of crystallinity on the Coulomb gap is minimal. Verification of this picture will require further experiments.

Significantly, similar trends in carrier accumulation and transport just described for P3HT were observed in the other five thiophene-based semiconductors. The average EGT parameters obtained from the polythiophene semiconductors are summarized in **Table 1**. The side chain lengths of poly(3-alkylthiophenes) (P3ATs, Figure 1a) were varied from four, to eight, to ten -CH_2- units, and the results can be compared with those of P3HT, **Figure 4**. All of the thiophene semiconductors exhibited qualitatively similar I_D and I_G changes with respect to V_G; I_D and I_G peaked at V_G = −1.6 — −1.9 V, and a collapse in both I_D and I_G was observed at high V_G (see Figure S5, Supporting Information). More importantly, the charge fraction per ring at the mobility peak was almost identical at ≈0.14 hpr for each of the thiophene-based semiconductors, Figure 4a,b. It is noteworthy that in previous studies the P3HT semiconductor gated with different electrolytes such as 1-ethyl-3-methylimidazolium fluoroalkylphosphate [EMI][FAP] or 0.1 M tetrabutylammonium hexafluorophosphate [TBA][HFP] in acetonitrile also showed maximum conductivity or mobility at similar charge density values of ≈10^{21} cm^{-3}.[23,45] This indicates that the optimal hole concentration for transport in polythiophenes is not affected by the side-chain architecture or the type of electrolyte ions. Additionally, note that the volumetric hole densities at maximum mobility (red trace in Figure 4a) were not the same across the polymer series because the number of thiophene rings in the semiconductor films per unit volume (i.e., the ring density) decreased with increasing side chain length, Figure 4a.[46,47]

Importantly, the maximum mobility increased with increasing alkyl side chain length, Figure 4b. Maximum mobility values were 0.24 ± 0.04, 0.61 ± 0.02, 0.68 ± 0.03, and 0.81 ± 0.03 cm^2 V^{-1} s^{-1} for P3BT, P3HT, P3OT, and P3DT, respectively, Table 1. This trend in mobility is essentially opposite to that observed in conventional organic field effect transistors (OFETs) in which longer insulating side chain lengths are thought to impede intramolecular charge transfer and have been reported to reduce crystalline order.[48] The increase in mobility of the polythiophenes with long alkyl chains in the electrolyte gating experiments is probably due to weaker hole-anion interaction, brought about by steric hindrance as discussed in the Introduction, which then lessens the localization of carriers. For example, hole carriers induced in P3BT with short side chains experience stronger attractive anion-hole interactions because of the shorter average distance between the anion and the thiophene backbone compared to polymers with longer alkyl side chains, Figure 4d.

Also, the difference in V_G at the I_D peaks between the forward and reverse sweeps, i.e., the peak voltage hysteresis, supports the presence of stronger hole-anion interactions in the thiophene polymers with shorter alkyl side chains. Figure 4c plots the peak voltage hysteresis versus side-chain length; the specific hysteresis values are also displayed in Table 1. From the shortest (butyl) to the longest (decyl) side chains the hysteresis systematically decreases by 130 mV. We propose that the I_D peak on the reverse scan of the I_D–V_G characteristic is shifted positively because of hole-anion interactions that stabilize polaronic holes on the polymer chains and make electrochemical de-doping difficult, leading to voltage hysteresis. The observation that longer side chains reduce the hysteresis is consistent with this concept as the longer side-chains should reduce, on average, the hole-anion interaction because of increased steric repulsion of the anions. We propose that these same hole-anion interactions are responsible for the lower peak height on the reverse sweep as well.

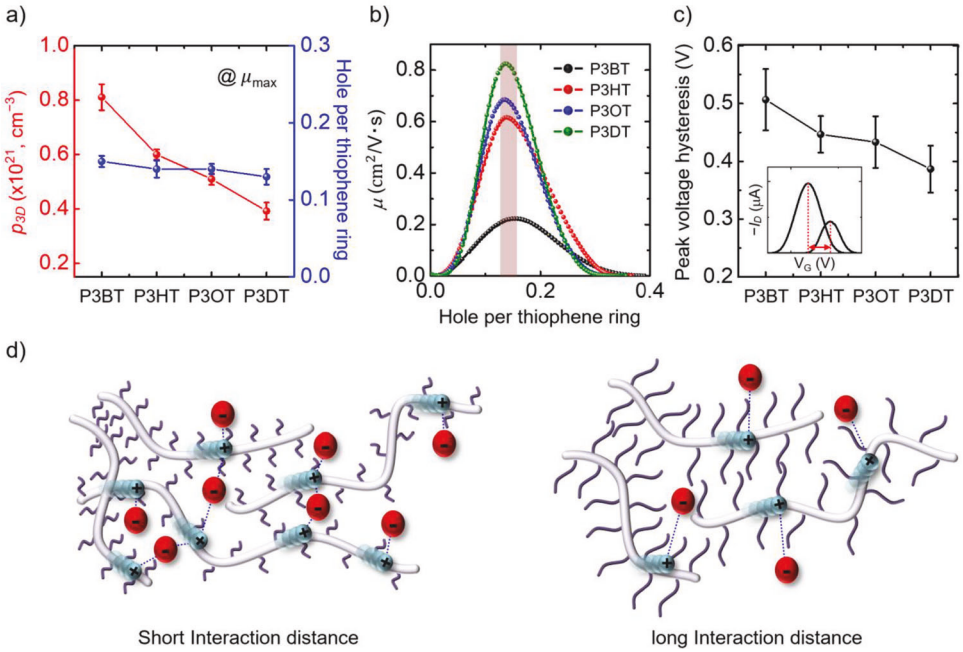

Figure 4. a) Average volumetric hole density and hole per thiophene ring (hpr) at maximum average mobility for each of the 4 P3AT semiconductors. b) Average charge carrier mobility as a function of calculated hpr for each of the 4 P3AT materials. c) I_D peak voltage hysteresis for the P3AT materials. Inset to (c) shows the definition of peak hysteresis in an $I_D - V_G$ plot. Error bars represent one standard deviation based on three devices. d) Schematics showing the relatively strong (short distance, left) and weak (long distance, right) interactions between the holes and ions of the thiophene-based semiconductors with short and long alkyl side chains, respectively.

In this context, the PBTTT and PQT polymer semiconductors represent interesting cases because their dodecyl (C_{12}) side chains are longer than any of the P3AT polymers just discussed, but their side-chain densities are approximately half that of the P3ATs. **Figure 5** shows their corresponding I_D–V_G, I_G–V_G, and μm-V_G behaviors. Overall, the results are very similar to the P3ATs: pronounced peaks are evident in both the I_D–V_G and I_G–V_G characteristics, with hysteresis on the reverse V_G sweeps, and the peak mobility again occurs near 0.14 hpr (actually at 0.13 and 0.12 hpr for PBTTT and PQT, respectively, Table 1), with essentially complete suppression of I_D and V_G at ~0.34 hpr. Notably, the peak hole mobility values of the PBTTT and PQT were

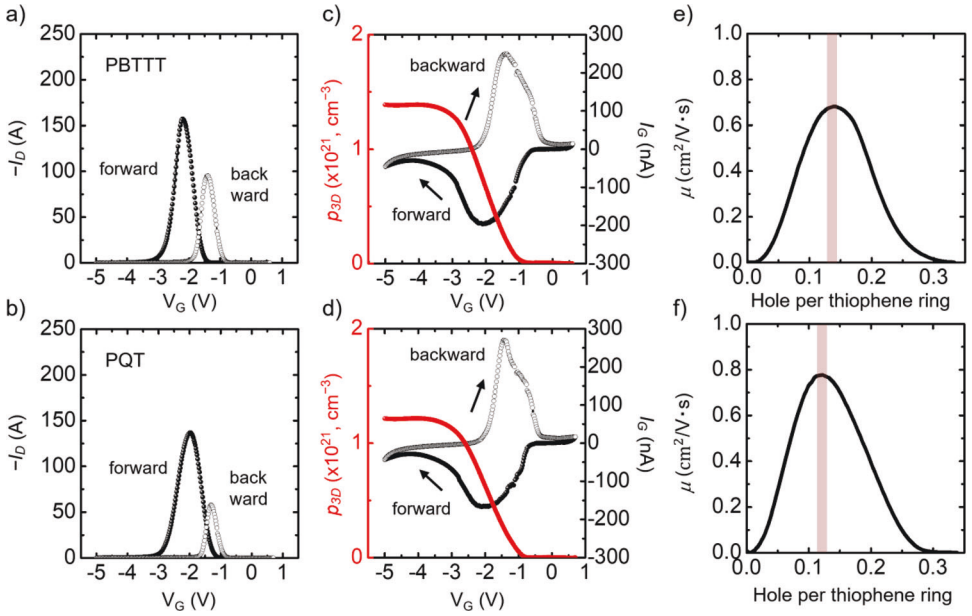

Figure 5. a,b) I_D-V_G transfer curves for PBTTT and PQT EGTs. c,d) are the corresponding I_G-V_G charging curves and the volumetric charge density (red) as a function of V_G. e,f) show the average charge carrier mobility versus hole per thiophene ring (hpr). V_G sweep rate was 50 mV s^{-1}.

Table 1. ON/OFF current ratio, threshold voltage (V_{th}), subthreshold swing (*SS*), peak voltage hysteresis, maximum mobility, volumetric charge density, and holes per thiophene ring (hpr) (at maximum mobility and shut-off) for the thiophene-based polymer semiconductors used in this study. Each parameter was calculated from three devices. Uncertainties represent one standard deviation.

Polymer	ON/OFF ratio	V_{th} [V]	*SS* [mV dec^{-1}]	Peak voltage hysteresis [V]	μm_{ax} [cm^2 V^{-1} s^{-1}]	p_{3D} at μm_{ax} [$\times 10^{21}$, cm^{-3}]	hpr at μm_{ax}	hpr at shut-off
P3BT	4.35 ± 1.15 ×10^3	−1.03 ± 0.04	226 ± 14	0.51 ± 0.05	0.24 ± 0.04	0.81 ± 0.05	0.15 ± 0.01	0.38 ± 0.02
P3HT	1.28 ± 0.14 ×10^4	−1.06 ± 0.02	197 ± 9	0.45 ± 0.03	0.61 ± 0.02	0.60 ± 0.02	0.14 ± 0.01	0.37 ± 0.01
P3OT	1.38 ± 0.14 ×10^4	−1.09 ± 0.03	176 ± 8	0.43 ± 0.04	0.68 ± 0.03	0.51 ± 0.02	0.14 ± 0.01	0.37 ± 0.01
P3DT	1.53 ± 0.13 ×10^4	−1.20 ± 0.04	143 ± 10	0.38 ± 0.04	0.81 ± 0.03	0.39 ± 0.03	0.13 ± 0.01	0.35 ± 0.01
PBTTT	3.61 ± 0.21 ×10^4	−1.48 ± 0.06	185 ± 16	0.76 ± 0.06	0.74 ± 0.06	0.58 ± 0.06	0.13 ± 0.02	0.34 ± 0.03
PQT	2.22 ± 0.08 ×10^4	−1.25 ± 0.03	194 ± 9	0.68 ± 0.04	0.77 ± 0.02	0.52 ± 0.03	0.12 ± 0.01	0.32 ± 0.01

0.74 ± 0.06 and 0.77 ± 0.02 cm^2 V^{-1} s^{-1}, respectively, which are higher than those of P3BT, P3HT, and P3OT and similar to that of P3DT (0.81 ± 0.03 cm^2 V^{-1} s^{-1}). This observation might reflect the intrinsically higher mobilities for PBTTT and PQT semiconductors reported in the literature, which has been ascribed to either higher crystallinity and/or flatter chain conformations that both promote carrier delocalization.[49–52] However, the higher mobilities appear to be somewhat at odds with the hysteresis observed for PBTTT and PQT. Average I_D–V_G hysteresis values for PBTTT and PQT are 0.76 ± 0.06 V and 0.68 ± 0.04 V, respectively, far higher, by up to 380 mV, than observed for the P3AT polymers (see P3DT vs PBTTT, Table 1). We believe that the large hysteresis for PBTTT and PQT makes sense: hole-ion interactions should be stronger in PBTTT and PQT because the alkyl side chain density is lower and therefore the ions can come into closer proximity with polaronic holes in the polymer backbones.

To reconcile the observation that peak mobility is higher for PBTTT and PQT versus the P3AT polymers, but that the hysteresis is larger, we hypothesize that hole-anion interactions do not "turn on" or become significant, until charge densities of ≈0.15 hpr are achieved. In fact, we have observed that indeed the hysteresis in the I_D–V_G and I_G–V_G traces is much reduced if V_G is only scanned out to the values corresponding to the I_D peak, Figure S6 (Supporting Information), which suggests that anion-hole interaction and the corresponding hysteresis only becomes active beyond a threshold charge density (i.e., the density at peak conductivity). Additionally, the decrease in hole mobility beyond the I_D peak also indicates an increase in hole-anion interactions. We believe this is an important point, which is under further investigation and will be more fully examined in a subsequent report. In general, our collective results on PBTTT, PQT, and P3AT polymers indicate that conductivity peaks and charging peaks are ubiquitous in EGTs that use polythiophene semiconductors. The collective results are also consistent with the picture that these peaks arise from filling of a polaronic sub-band at ≈0.38 hpr, arising from strong hole-anion Coulombic interactions.

3. Conclusion

In summary, we systematically investigated carrier accumulation, localization, and transport phenomena in electrochemically-gated thiophene-based polymer semiconductors over a wide voltage range up to $V_G = -5$ V. We observed that the channel current I_D and gate current I_G initially increase with increasing V_G, reach maximum values, and subsequently decrease at higher (more negative) V_G. Complete shut-off of carrier accumulation and conductivity occur beyond $V_G = -3$ V, which corresponds to 0.32 – 0.38 hpr. We posit that the cause of this behavior is strong anion-hole Coulombic interactions which split the HOMO bands of the polymers into upper and lower sub-bands; filling the upper sub-band at hole densities of 0.32 – 0.38 hpr results in a collapse in the conductivity and hole mobility. The observed increase in conductivity and average peak mobility with increasing alkyl side chain lengths on the polymers is consistent with this picture; longer side chains provide increasing steric barriers between the pi-conjugated polymer backbones and anions, yielding weaker hole-anion interactions. The observed conductivity hysteresis and its dependence on side-chain lengths and side-chain densities is also consistent with this view. Overall, our results

suggest that ion-carrier interactions are of crucial importance in electrochemically doped polymers; polymer and electrolyte designs that minimize Coulombic interactions should lead to enhanced transport in conjugated polymer semiconductors.

4. Experimental Section

Materials: [BMI][FAP] ionic liquid (IL) was purchased from Merck. PBTTT, PQT, and terpineol were purchased from Sigma-Aldrich. Regioregular poly(3-alkylthiophenes) (P3AT) with butyl (P3BT), hexyl (P3HT), octyl (P3OT), or decyl (P3DT) side chains were purchased from Rieke Metals. PEDOT:PSS (Clevios PH 1000) was purchased from Heraeus. Chloroform and ethyl acetate were purchased from Thermo Fisher. All materials were used as received.

Ink Preparation for Aerosol-Jet-Printing: Semiconductor inks (P3BT, P3HT, P3OT, P3DT, PBTTT, and PQT) were prepared by dissolving a polymer semiconductor in chloroform at a concentration of 1 mg mL^{-1} and then terpineol (chloroform : terpineol = 9:1 by volume) was added before printing. An ionogel ink was obtained by blending SEAS triblock polymer, [BMI][FAP], and ethyl acetate at a mass ratio of 1:9:90. The SEAS triblock co-polymer was synthesized in-house by a previously reported procedure and used as the gelating polymer network of the ionogel.[35] For the PEDOT:PSS ink, 5 wt.% of ethylene glycol was mixed with an aqueous PEDOT:PSS solution. All precursor solutions were stirred at a hotplate temperature of 50 °C for more than 2 h before use.

Device Fabrication and Characterization: For top-gated EGTs, 5 nm Cr and 45 nm Au source (*S*) and drain (*D*) electrodes separated by a channel length (*L*) of 100 µm and channel width (*W*) of 1000 µm were patterned on a SiO_2 substrate via metal evaporation through a stencil mask. For side-gated EGTs that utilized a gold gate electrode instead of PEDOT:PSS, the Au/Cr source and drain electrodes were patterned onto a SiO_2 wafer by photolithography. In both cases, an electron beam evaporator (CHA SEC-600) was used to evaporate Cr and Au. To complete the devices, thiophene-based polymer, ionogel, and PEDOT:PSS inks were deposited sequentially under ambient air conditions with an AJ 200 benchtop aerosol jet printer (Optomec, Inc.) to form the semiconductor channel, electrolyte dielectric, and gate electrode, respectively. The stage temperature was maintained at 60 °C during printing to evaporate any residual solvent. A 150-µm nozzle was employed to print the polymer semiconductor and PEDOT:PSS layers. A 200-µm nozzle was used for the ionogel. The carrier (N_2) and sheath gas (N_2) flow rates (sccm) for the semiconductor, ionogel, and PEDOT:PSS were 15/20, 25/30, and 30/40, respectively. The atomizer current was kept at ≈0.25, ≈0.35, and ≈0.45 A to print the semiconductor, ionogel, and PEDOT:PSS, respectively. The average thickness of the printed semiconductors and PEDOT:PSS, measured using a KLA P-7 surface profiler, was 52 ± 7 nm and ~3 µm, respectively. The fabricated EGTs were examined using a Desert Cryogenics (Lakeshore) probe station with a Keithley 236 source meter and Keithley 6517A electrometers in an N_2-filled glovebox at room temperature. I_G was measured at the gate electrode while applying V_G, simultaneously. The induced hole density (Q) was extracted from gate current-gate voltage (I_G–V_G) curves on the forward sweep:[23]

$$Q = \frac{\int I_G dV}{r_V} \tag{1}$$

where r_V denotes the V_G sweep rate. A specific charge density at a certain V_G was extracted by integrating the I_G–V_G curve in the forward sweep up to that specific V_G. To obtain accurate hole density, the integration of I_G was conducted excluding the baseline consisting of parasitic capacitive and leakage currents (see Figure 2c). From the hole density Q, the volumetric hole density (p_{3D}) was calculated using the following equation:[23]

$$p_{3D} = \frac{Q}{eAt_{film}} \tag{2}$$

where e is the elementary charge, and A and t_{film} are the area and thickness of the aerosol-jet-printed semiconductor films, respectively. The average hole mobility (μ) was obtained using the following equation with area-normalized hole density ($p_A = Q/A$):[53]

$$\mu = \frac{L}{W}\frac{I_D}{ep_A V_D} \tag{3}$$

where L and W are the channel lengths and widths, and V_D is the drain voltage. The charge density expressed as holes per thiophene ring (hpr) was estimated by the following equation:[23]

$$hpr = \frac{p_{3D} V_{cell}}{Number\ of\ thiophene\ ring/unit\ cell} \tag{4}$$

where V_{cell} is the volume of the crystalline unit cell and the number of thiophene rings in each unit cell is four. Note that the thieno[3,2-*b*]thiophene subunit of PBTTT was considered to count as two thiophene rings. In this study, semiconductor films were expected to be mostly amorphous because additional thermal/solvent annealing processes were not applied to induce crystallinity and penetration of ions is known to disrupt crystallinity.[20] Thus, the hpr values calculated by the aforementioned equations are likely underestimated by up to 10–15% because the crystalline domain is typically 10−15% more dense than the amorphous domain in the semicrystalline polymers.[54]

Supporting Information

Supporting Information is available from the Wiley Online Library or from the author.

Acknowledgements

This research was financially supported by the National Research Foundation of Korea (NRF) grant funded by the Korean government (Ministry of Science and ICT, MSIT) (2021R1A2C1094911), Korea Basic Science Institute (National research Facilities and Equipment Center) grant funded by the Ministry of Education (2021R1A6C101A404) and the Korea Institute for Advancement of Technology (KIAT), and the Ministry of Trade, Industry & Energy (MOTIE) of the Republic of Korea (No. P0017363). This work was also partially supported by the MRSEC program of the U.S. National Science Foundation (NSF) under Grant Number DMR-2011401. Portions of this work were conducted in the Minnesota Nano Center, which was also supported by NSF through the NNCI Network under Award Number ECCS-2025124. D.Z.A. acknowledges support from the Michael H. Baker Family Foundation.

Conflict of Interest

The authors declare no conflict of interest.

Data Availability Statement

The data that support the findings of this study are available from the corresponding author upon reasonable request.

Keywords

carrier localization, charge transports, electrolyte-gated transistors, polaron, sub-band filling, thiophene polymers

Received: April 3, 2023
Revised: May 1, 2023
Published online: May 18, 2023

[1] F. Torricelli, D. Z. Adrahtas, Z. N. Bao, M. Berggren, F. Biscarini, A. Bonfiglio, C. A. Bortolotti, C. D. Frisbie, E. Macchia, G. G. Malliaras, I. McCulloch, M. Moser, T. Q. Nguyen, R. M. Owens, A. Salleo, A. Spanu, L. Torsi, *Nat. Rev. Method. Prim.* **2021**, *1*, 66.
[2] C. Leighton, *Nat. Mater.* **2019**, *18*, 13.
[3] P. Gkoupidenis, D. A. Koutsouras, G. G. Malliaras, *Nat. Commun.* **2017**, *8*, 15448.
[4] S. H. Kim, K. Hong, W. Xie, K. H. Lee, S. P. Zhang, T. P. Lodge, C. D. Frisbie, *Adv. Mater.* **2013**, *25*, 1822.
[5] K. G. Cho, K. H. Seol, M. S. Kim, K. H. Y. Hong, K. H. Lee, *ACS Appl. Mater. Interfaces* **2022**, *14*, 50004.
[6] T. He, C. D. Frisbie, *ACS Nano* **2022**, *16*, 4823.
[7] L. Q. Flagg, R. Giridharagopal, J. J. Guo, D. S. Ginger, *Chem. Mater.* **2018**, *30*, 5380.
[8] Y. Na, F. S. Kim, *Chem. Mater.* **2019**, *31*, 4759.
[9] D. H. Ho, D. G. Roe, Y. Y. Choi, S. Kim, Y. J. Choi, D. Kim, S. B. Jo, J. H. Cho, *Sci. Adv.* **2022**, *8*, eabn1838.
[10] S. Lee, H. J. Lee, Y. Ji, K. H. Lee, K. Hong, *Adv. Mater.* **2021**, *33*, 2005456.
[11] B. D. Paulsen, K. Tybrandt, E. Stavrinidou, J. Rivnay, *Nat. Mater.* **2020**, *19*, 13.
[12] J. Chung, A. Khot, B. M. Savoie, B. W. Boudouris, *ACS Macro Lett.* **2020**, *9*, 646.
[13] S. I. Rich, R. J. Wood, C. Majidi, *Nat. Electron.* **2018**, *1*, 102.
[14] N. A. Kukhta, A. Marks, C. K. Luscombe, *Chem. Rev.* **2022**, *122*, 4325.
[15] L. S. Hornberger, D. Neusser, C. Malacrida, L. G. Kaake, S. Ludwigs, *Appl. Phys. Lett.* **2021**, *119*, 163301.
[16] D. Neusser, C. Malacrida, M. Kern, Y. M. Gross, J. van Slageren, S. Ludwigs, *Chem. Mater.* **2020**, *32*, 6003.
[17] Y. Yamashita, J. Tsurumi, M. Ohno, R. Fujimoto, S. Kumagai, T. Kurosawa, T. Okamoto, J. Takeya, S. Watanabe, *Nature* **2019**, *572*, 634.
[18] M. Fahlman, S. Fabiano, V. Gueskine, D. Simon, M. Berggren, X. Crispin, *Nat. Rev. Mater.* **2019**, *4*, 627.
[19] L. Q. Flagg, C. G. Bischak, J. W. Onorato, R. B. Rashid, C. K. Luscombe, D. S. Ginger, *J. Am. Chem. Soc.* **2019**, *141*, 4345.
[20] J. O. Guardado, A. Salleo, *Adv. Funct. Mater.* **2017**, *27*, 1701791.
[21] T. L. Atallah, M. V. Gustafsson, E. Schmidt, C. D. Frisbie, X. Y. Zhu, *J. Phys. Chem. Lett.* **2015**, *6*, 4840.
[22] B. D. Naab, X. D. Gu, T. Kurosawa, J. W. F. To, A. Salleo, Z. A. Bao, *Adv. Electron. Mater.* **2016**, *2*, 1600004.
[23] B. D. Paulsen, C. D. Frisbie, *J. Phys. Chem. C* **2012**, *116*, 3132.
[24] S. Wang, M. J. Ha, M. Manno, C. D. Frisbie, C. Leighton, *Nat. Commun.* **2012**, *3*, 1210.
[25] M. J. Panzer, C. D. Frisbie, *J. Am. Chem. Soc.* **2007**, *129*, 6599.
[26] D. Ofer, M. S. Wrighton, *J. Am. Chem. Soc.* **1988**, *110*, 4467.
[27] D. Ofer, R. M. Crooks, M. S. Wrighton, *J. Am. Chem. Soc.* **1990**, *112*, 7869.
[28] W. Xie, S. Wang, X. Zhang, C. Leighton, C. D. Frisbie, *Phys. Rev. Lett.* **2014**, *113*, 246602.
[29] M. J. Panzer, C. D. Frisbie, *J. Am. Chem. Soc.* **2005**, *127*, 6960.
[30] P. C. Harikesh, C. Y. Yang, H. Y. Wu, S. L. Zhang, M. J. Donahue, A. S. Caravaca, J. D. Huang, P. S. Olofsson, M. Berggren, D. Tu, S. Fabiano, *Nat. Mater.* **2023**, *22*, 242.
[31] K. Xu, T. P. Ruoko, M. Shokrani, D. Scheunemann, H. Abdalla, H. D. Sun, C. Y. Yang, Y. Puttisong, N. B. Kolhe, J. S. M. Figueroa, J. O. Pedersen, T. Ederth, W. M. Chen, M. Berggren, S. A. Jenekhe, D. Fazzi, M. Kemerink, S. Fabiano, *Adv. Funct. Mater.* **2022**, *32*, 2112276.
[32] I. Salzmann, G. Heimel, M. Oehzelt, S. Winkler, N. Koch, *Accounts Chem. Res.* **2016**, *49*, 370.
[33] R. Q. Png, M. C. Y. Ang, M. H. Teo, K. K. Choo, C. G. Tang, D. Belaineh, L. L. Chua, P. K. H. Ho, *Nat. Commun.* **2016**, *7*, 11948.
[34] P. J. Chia, S. Sivaramakrishnan, M. Zhou, R. Q. Png, L. L. Chua, R. H. Friend, P. K. H. Ho, *Phys. Rev. Lett.* **2009**, *102*, 096602.
[35] B. X. Tang, S. P. White, C. D. Frisbie, T. P. Lodge, *Macromolecules* **2015**, *48*, 4942.
[36] N. De Vos, C. Maton, C. V. Stevens, *ChemElectroChem* **2014**, *1*, 1258.
[37] A. M. O'Mahony, D. S. Silvester, L. Aldous, C. Hardacre, R. G. Compton, *J. Chem. Eng. Data* **2008**, *53*, 2884.
[38] M. Galinski, A. Lewandowski, I. Stepniak, *Electrochim. Acta* **2006**, *51*, 5567.
[39] M. P. S. Mousavi, B. E. Wilson, S. Kashefolgheta, E. L. Anderson, S. Y. He, P. Buhlmann, A. Stein, *ACS Appl. Mater. Interfaces* **2016**, *8*, 3396.
[40] J. Rivnay, P. Leleux, M. Ferro, M. Sessolo, A. Williamson, D. A. Koutsouras, D. Khodagholy, M. Ramuz, X. Strakosas, R. M. Owens, C. Benar, J. M. Badier, C. Bernard, G. G. Malliaras, *Sci. Adv.* **2015**, *1*, e1400251.
[41] C. Wakai, A. Oleinikova, M. Ott, H. Weingartner, *J. Phys. Chem. B* **2005**, *109*, 17028.
[42] J. Brebels, J. V. Manca, L. Lutsen, D. Vanderzande, W. Maes, *J. Mater. Chem. A* **2017**, *5*, 24037.
[43] X. Liu, K. S. Jeong, B. P. Williams, K. Valchshouri, C. H. Guo, K. Han, E. D. Gomez, Q. Wang, J. B. Asbury, *J. Phys. Chem. B* **2013**, *117*, 15866.
[44] B. Neelamraju, M. Rudolph, E. L. Ratcliff, *J. Phys. Chem. C* **2018**, *122*, 21210.
[45] Z. T. Chen, E. L. Ratcliff, *Chem. Mater. 34*, 10691.
[46] K. Tashiro, K. Ono, Y. Minagawa, M. Kobayashi, T. Kawai, K. Yoshino, *J. Polym. Sci., Part B: Polym. Phys.* **1991**, *29*, 1223.
[47] J. Corish, D. A. MortonBlake, F. Beniere, M. Lantoine, *J. Chem. Soc., Faraday Trans.* **1996**, *92*, 671.
[48] Y. D. Park, D. H. Kim, Y. Jang, J. H. Cho, M. Hwang, H. S. Lee, J. A. Lim, K. Cho, *Org. Electron.* **2006**, *7*, 514.
[49] S. Himmelberger, J. Dacuna, J. Rivnay, L. H. Jimison, T. McCarthy-Ward, M. Heeney, I. McCulloch, M. F. Toney, A. Salleo, *Adv. Funct. Mater.* **2013**, *23*, 2091.
[50] C. C. Wang, L. H. Jimison, L. Goris, I. McCulloch, M. Heeney, A. Ziegler, A. Salleo, *Adv. Mater.* **2010**, *22*, 697.
[51] M. L. Chabinyc, L. H. Jimison, J. Rivnay, A. Salleo, *MRS Bull.* **2008**, *33*, 683.
[52] I. McCulloch, M. Heeney, C. Bailey, K. Genevicius, I. Macdonald, M. Shkunov, D. Sparrowe, S. Tierney, R. Wagner, W. M. Zhang, M. L. Chabinyc, R. J. Kline, M. D. McGehee, M. F. Toney, *Nat. Mater.* **2006**, *5*, 328.
[53] H. M. Yang, Y. K. Kwon, S. B. Lee, S. Kim, K. Hong, K. H. Lee, *ACS Appl. Mater. Interfaces* **2017**, *9*, 8813.
[54] G. W. Ehrenstein, *Polymeric materials: structure, properties, applications*, Carl Hanser Verlag GmbH Co KG, Munich, Germany **2012**.